Investigating the role of drug transporters in furosemide absorption, food-effect and elimination by a proteomics informed-mechanistic PBPK modeling approach

Revathi Chapa

A thesis

submitted in partial fulfillment of the

requirements for the degree of

Master of Science

University of Washington

2019

Committee:

Bhagwat Prasad

Qingcheng Mao

Program Authorized to Offer Degree:

Pharmaceutics

University of Washington

Abstract

Investigating the role of drug transporters in furosemide absorption, food-effect and elimination by a proteomics informed-mechanistic PBPK modeling approach

Revathi Chapa

Chair of the Supervisory Committee: Bhagwat Prasad, Department of Pharmaceutics

Abstract:

Furosemide is a widely used diuretic for treating excessive fluid accumulation caused by disease conditions like heart failure and liver cirrhosis. Furosemide exhibits variable pharmacokinetics (PK) with bioavailability ranging from 10-100%, which is attributed to its low solubility and low permeability. Furosemide also shows moderate negative food effect despite of its higher solubility in fed-condition. To explain these clinical observations, we hypothesized that transporter mediated permeability plays a significant role in variable absorption, food effect and elimination of furosemide. To test this, we i) characterized the role of intestinal efflux transporters in furosemide absorption including food-effect and ii) predicted the contribution of renal uptake and efflux transporters on its disposition by using a proteomics-informed mechanistic physiologically based pharmacokinetic (PBPK) modeling. Our *in vitro* results confirmed that furosemide is a substrate of various intestinal transporters, i.e., BCRP, MRP4 and OATP2B1. The PBPK model suggests that fasting condition leads to saturation of BCRP because of the faster gastric emptying. On the other hand, delayed gastric emptying allows efficient BCRP mediated furosemide efflux in fed condition, hence explains the negative food effect. The study could be further extended to test the effect of BCRP, MRP4 and OATP2B1 genetic polymorphisms or drug-interactions on absorption, disposition, efficacy and toxicity of furosemide. Further, as furosemide has been proposed as a probe substrate of renal organic anion transporters (OATs) for assessing clinical drug-drug interactions (DDIs) during drug development, the confounding effects of intestinal transporters on furosemide PK should be considered while interpreting such clinical transporter DDI studies.

Acknowledgements

I would like to express my deep gratitude to my advisor Dr. Bhagwat Prasad, for his years of guidance and mentorship at the University of Washington, without his support I would not be where I am today. I would also like to thank my reading committee Dr. Qingcheng Mao, for his time and interest in my work.

I would like to express my appreciation towards Dr. Arzu Selen, for her scientific input and the mentorship.

Lastly, I would like to thank the faculty, staff, and the students of the Pharmaceutics department for all their support and lasting friendship.

Table of Contents Page

LIST OF FIGURES

LIST OF SUPPLEMENTARY FIGURES

LIST OF TABLES

LIST OF SUPPLEMENTARY TABLES

ABBREVIATIONS

AMP: adenosine 5’-monophosphate

ATP: adenosine 5’-triphosphate

AUC: area under the curve

B/P: blood to plasma partition

BCRP: breast cancer resistance protein

BCS: biopharmaceutics classification system

BSA: bovine serum albumin

Caco-2: colorectal adenocarcinoma

CLint: intrinsic clearance

CLiv: in vivo clearance;

CLr: renal clearance

Cmax: maximum plasma concentration

DMEM: dulbecco’s modified eagle's medium

DDI: drug-drug interaction

FDA: food and drug administration

F_a = fraction available from dosage form

F_e: fraction excreted

F_m: fraction metabolized

F_u: fraction unbound

HBSS: hanks balanced salt solution

PBS: phosphate buffer saline

ISEF: inter system extrapolation factor

Jmax: in vitro maximum rate of transporter-mediated efflux or uptake

Ka: absorption rate constant

Ki: concentration of inhibitor that supports half maximal inhibition

Km: michaelis-menten constant

LogP: partition coefficient

MAT: mean absorption time

M-ADAM: multi-layer gut wall advanced dissolution absorption and metabolism

MDCK-II: madin-darby canine kidney-II

MDT: mean dissolution time

MRP2: multidrug resistance-associated protein 2

MRP3: multidrug resistance-associated protein 3

MRP4: multidrug resistance-associated protein 4

MRT: mean residence time

OATP1B1: organic anion transporting polypeptide 1B1

OATP1B3: organic anion transporting polypeptide 1B3

OATP2B1: organic anion transporting polypeptide 2B1

OAT1: organic anion transporter 1

OAT3: organic anion transporter 3

P_{app}: apparent permeability in caco-2

PBPK: physiologically based pharmacokinetic

P_{eff}: effective permeability in human

P-gp: P-glycoprotein

PK: pharmacokinetics

PKa: acid dissociation constant

RAF: relative activity factor

UGT: uridine diphosphate-glucuronosyltransferase

Vss: volume at steady state

1. INTRODUCTION

Furosemide is one of the most commonly used loop diuretics,[1] which continues to be an important first-line drug in the treatment of edema associated with kidney impairment, liver cirrhosis, hypertension and chronic heart failure.[2,3] It acts by blocking Na^+-K^+-$2Cl^-$ cotransporter in the thick ascending limb of the loop of Henle, thus causing excessive excretion of water along with sodium, chloride, and potassium.[4–6] Although furosemide is generally safe and routinely prescribed to adult as well as pediatric patients,[2,3,7–10] in the normal dose ranges (i.e., 600 mg/day in adults, and 0.5 to 2 mg/kg/dose every 6 to 24 hours in pediatrics),[11–13] if given in higher dosing, it can lead to profound water and electrolyte depletion, and in some cases leading to potential toxic effects like ototoxicity.[14–19] Therefore, the food and drug administration (FDA) label recommends a careful medical monitoring to adjust the dose and dosing schedule according to the need of individual patients.[20]

The average bioavailability of furosemide is ~60%,[21–23] however it is highly variable and can range from 10-100% with significant inter- and intra-subject variability.[2] Such erratic drug absorption is generally caused by factors that influence solubility and/or permeability, such as differences in pH, dosage form, gastric emptying, food intake, efflux transporter activity, etc. Majority of furosemide dose is eliminated renally through active secretion ($f_e \sim 65\%$) primarily mediated by organic anion transporters (OATs), i.e., OAT1 and OAT3 in concert with MRP4, and the rest by UGT1A9-mediated metabolism ($f_m \sim 35\%$).[2,24–26] Furosemide is practically insoluble in water and acidic pH, i.e., solubility <0.1 mg/mL,[27] however, its solubility is >20-100-fold greater in intestinal pH at ~6.8, thus allowing complete dissolution of 40 or 80 mg tablet dose in intestinal fluid.[28] Chemical degradation in the gastric pH is another factor that can influence drug absorption, however, this has been ruled out as a contributor to the poor

bioavailability.[29] On the other hand, permeability of furosemide determined using *in vitro* systems is poor i.e., $P_{app} \leq 2.0 \times 10^{-6}$ cm/sec.[30,31] In general, drug permeability can be influenced by efflux or uptake transporters besides passive diffusion. High basolateral to apical permeability in comparison to apical to basolateral permeability in Caco-2 monolayers,[32] and exercised rat jejunum model,[33] has been reported indicating that it is a substrate of efflux transporter(s). However, the contribution of individual intestinal transporters such as organic anion transporters (e.g., OATP2B1), P-glycoprotein (P-gp), breast cancer resistance protein (BCRP), multidrug resistance protein (MRP) is unknown. Therefore, the first aim of this study was to identify the intestinal efflux and uptake transporters that would govern furosemide absorption using membrane vesicles and transfected cells *in vitro*. We then characterized the kinetic parameters (J_{max} and K_m), and also quantified the transporter abundance in vesicles and cells using quantitative proteomics.

Furosemide exhibits negative food effect, i.e., a significant reduction in the rate (higher C_{max} and delayed t_{max}) and extent (area under the curve, AUC) when compared to fasting conditions.[23,34,35] However, these in vivo observations do not correlate with dissolution data conducted in fed-state simulated gastric fluid.[36] Thus, we hypothesized that negative food effect observed for furosemide is a consequence of interplay between gastric emptying and intestinal efflux transport of furosemide, i.e., the delayed gastric emptying in fed condition would result in efficient efflux because the transporter is not saturated unlike in the fasting condition. To test this hypothesis, we developed a mechanistic middle-out whole-body physiologically based pharmacokinetic (PBPK) model describing the intravenous and oral pharmacokinetics (PK) of furosemide in healthy adults by integrating physico-chemical, *in vitro* dissolution, metabolism, transport and excretion parameters using Simcyp (Certara, Princeton, NJ). We also investigated the effect of food

induced delayed gastric emptying on PK of furosemide. Finally, a thorough sensitivity analysis was performed to predict effect of apical uptake, efflux and basolateral efflux, and gastric emptying on bioavailability. Although top-down PBPK models of furosemide were previously published,[36,37] our model is based on mechanistic middle-out approach, incorporating the key transporters to absorption and disposition of furosemide, with a goal of improving the prediction of transporter-mediated drug-drug interactions (DDIs) and food-effect.

2. EXPERIMENTAL

2.1 Materials

Membrane vesicles overexpressing the human BCRP, P-gp, MRP2, MRP3, MRP4 and stably transfected hOATP2B1-MDCK-II cells were procured from Solvo Biotechnology (Budapest, Hungary). Cell culture medium Dulbecco's modified Eagle's medium (DMEM), fetal bovine serum,1% GlutaMAX-1, 100 U/mL penicillin and 100 μg/streptomycin were obtained from Sigma-Aldrich (St. Louis, MO). Furosemide, diclofenac, estrone-3-sulfate, rosuvastatin, adenosine 5'-triphosphate (ATP) disodium salt, adenosine 5'-monophosphate (AMP) monohydrate, glutathione, tris [hydroxymethyl] aminomethane (tris-base), MgCl2, NaCl, sucrose, and 3-[N-morpholino] propane sulfonic acid (MOPS) were purchased from Sigma-Aldrich (St. Louis, MO). Bovine serum albumin (BSA), membrane protein extraction kit and trypsin digestion reagents were obtained from Thermo Fisher Scientific (Rockford, IL). Hanks balanced salt solution (HBSS), phosphate buffer saline (PBS), acetonitrile, formic acid were purchased from Thermo Fisher Scientific (Rockford, IL). The synthetic unlabeled and stable labeled peptides were purchased from New England Peptides (Boston, MA) and Thermo Fisher

Scientific (Rockford, IL), respectively. Multiscreen TM HTS Vacuum Manifold and 96-well filter plates with class B glass fiber filters were purchased from EMD Millipore (Billerica, MA).

2.2 Vesicular transport assay

A previously validated vesicular transport assay[38,39] was used to investigate efflux transporter mechanisms of furosemide. Briefly, the furosemide transport was studied using an initial screening assay employing vesicles overexpressing efflux transporters, i.e., BCRP, P-gp, MRP2, MRP3, and MRP4. The assay was carried out in 96-well polystyrene plates by incubating 10 µM furosemide with 4 mM ATP or AMP at 37 °C in the following assay buffers: i) 40 mM MOPS-Tris (pH 7.0), 70 mM KCl, and 7.5 mM $MgCl_2$ for MRP2, or ii) 10 mM Tris-HCl, 10 mM MgCl2, and 250 mM sucrose for one minute. Control membrane vesicles were also used to estimate passive diffusion. The transport was quenched by the addition of 200 µl of cold wash buffer (40 mM MOPS-Tris, pH 7.0, 70 mM KCl) and the solution was transferred to a 96-well filter plate. The filter plate was washed with 5 x 200 µl of ice-cold wash buffer under vacuum filtration. The substrate contained in the vesicles was eluted with 100 µl of 1:1 acetonitrile:0.2% formic acid containing internal standard (diclofenac, 500 nM) and subjected to LC-MS/MS analysis. The transport kinetic analyses were then carried out for the transporters that exhibited activity in the initial screening. The kinetic parameters (J_{max} and K_m) were derived from assay conducted using substrate concentration range of 1 to 100 µM at 37 °C for 30 seconds, and fitting into Michaelis-Menten equation. The functional transport activity of the vesicles was confirmed by using probe substrates (**Supplementary Table S1**).

2.3 Time- and concentration-dependent uptake of furosemide in hOATP2B1 transfected cells

The time course of furosemide uptake by OATP2B1-transfected MDCK-II cells was evaluated to determine the incubation time required for initial uptake rate estimates. Transport studies were initiated by seeding cells at a density of~2×10^5 cells per well in 24-well poly-D-lysine coated plates. Cells were grown in DMEM containing 10% fetal bovine serum and 0.1 mg/mL streptomycin. The cells were then incubated at 37 °C/5% CO_2 for 24 hours. Culture media was removed, and the cells were washed three times with PBS. After acclimatization in HBSS buffer for 10 min, cells were treated with furosemide for 2, 5, 10 and 15 min. Similarly, for the transport kinetics of furosemide, the uptake rate at varying concentrations (0.5-500 µM) was measured at 15 min and 37 °C in mock/OATP2B1-transfected MDCK-II cells. The cellular uptake was terminated by quickly removing drug solution and washing the cells three times with 500 µL of ice cold HBSS buffer. The cells were then lysed in 300 µL of 100% methanol containing internal standard for LC-MS/MS analysis or 0.1% Triton X100 for analyzing protein content. The samples were centrifuged at 3000 xg for 10 min and the cell supernatant was transferred to a 96-deep well plate for LC-MS/MS analysis. The functional transport activity of the hOATP2B1 transfected cells was confirmed initially by using probe substrates for OATP2B1, i.e., estrone-3-sulfate and rosuvastatin at 2 µM for 2 min (**Supplementary Fig. 1**). Mock-transfected MDCK-II cells were used as the control.

2.4 Quantification of efflux transporters in vesicles and transfected hOATP2B1-MDCK-II cells using quantitative LC-MS/MS proteomics

The total membrane proteins from hOATP2B1-transfected cells were isolated using optimized protocol.[40] The total protein content in the membrane samples was determined by using BCA protein assay kit (Pierce Biotechnology, Rockford, IL), which was diluted to a working

concentration of 2 mg/ml. 25 µg total vesicular protein (diluted to 80 µl) and 80 µg membrane protein of hOATP2B1-MDCK-II cells (diluted to 56 µl) were incubated with 10 µl of dithiothreitol (250 mM), 30 µl of ammonium bicarbonate buffer (100 mM, pH 7.8), 20 µl of BSA (0.02 mg/ml), and 10 µl of human serum albumin (10 mg/ml) at 95 °C for 10 min. After cooling down to room temperature, 20 µl of iodoacetamide (500 mM) was added to the mixture and incubated at room temperature for 30 min in the dark. To concentrate the sample, ice-cold methanol (0.5 ml), chloroform (0.1 ml), and water (0.4 ml) were added to each sample and thoroughly mixed by vortex. After centrifugation at 16,000 x g for 5 min at 4 °C, the pellet was washed once with ice-cold methanol (0.5 ml) and centrifuged at 8,000 xg for 5 min at 4 °C. The pellet was re-suspended with 60 µl of ammonium bicarbonate buffer (50 mM). Finally, the protein sample was digested with 20 µl of trypsin at 1:10 trypsin: protein ratio (w/w) and incubated for 16 h at 37 °C with mixing at 300 rpm. The digestion reaction was quenched by 20 µl of chilled stable-labeled peptide internal standard (dissolved in 80% acetonitrile with 0.5% formic acid) and centrifuged at 4,000 x g for 5 min at 4 °C. All samples were digested and processed in triplicates.

The surrogate peptides of BCRP, MRP4 and OATP2B1 were quantified in the digested samples using a validated LC-MS/MS method using SCIEX Triple Quadrupole 6500 system (Framingham, WA) coupled to an ACQUITY UPLC system (Waters Technologies, Milford, MA).[40,41] 5 µl of each sample was injected to the column (ACQUITY UPLC HSS T3 1.8 µm, C18 100A; 100 x 2.1 mm, Waters, Milford, MA). The chromatographic method was used with a gradient mobile phase (0.3 ml/min) consisted of 0.1% formic acid in water (A) and 0.1% formic acid in acetonitrile (B) (**Supplementary Table S2**). Unlabeled peptides represent analytes and the corresponding stable-labeled peptides were used as internal standards (**Supplementary**

Table S3). The pooled total membrane sample isolated from liver tissue with known transporter abundance was used as a calibrator for estimation of abundances of individual transporters in vesicles and cells. The calibration curve range and linearity were verified by serial dilutions of the studied transporter peptide standards. The LC-MS/MS data were analyzed by Skyline software.

2.5 LC-MS/MS analysis of furosemide

The amount of furosemide retained in the vesicles and MDCK-II cells was quantified by LC-MS/MS using SCIEX 6500 instrument (Framingham, WA) coupled to an ACQUITY UPLC system (Waters Technologies, Milford, MA). 5 µl of sample was injected to the column (ACQUITY UPLC HSS T3 1.8 µm, C18 100A; 100 x 2.1 mm, Waters, Milford, MA) using a gradient mobile phase (0.3 ml/min) consisted of 0.1% formic acid in water (A) and 0.1% formic acid in acetonitrile (B) (**Supplementary Table S4**).

2.6 Workflow of furosemide PBPK model and model evaluation

A simplified PBPK workflow of furosemide PK is presented in **Supplementary Fig. 2**. Individual steps are detailed in the following section.

a. Development of intravenous (IV) PBPK model in healthy adults

A whole body mechanistic PBPK model of furosemide was developed in a virtual north European Caucasian population using the population-based simulation software Simcyp simulator Ver. 17 (Certara, Princeton, NJ). A total of 80 virtual individuals (10 trials × 8 individuals), aged between 25 and 50years, with an equal proportion of males and females, and were used across all simulations. The virtual study design was defined as close as possible to those in the original clinical studies.

The PBPK model development and validation consisted of the two steps. First, the PBPK model of furosemide following intravenous administration (IV) was developed using the physicochemical, biopharmaceutical, and pharmacokinetic parameters obtained from extensive literature search.[21,23,25,42–46] Detailed input parameters for model development are summarized in **Table 1**. A full PBPK model based on the method established by Rodgers and Rowland was used for the prediction of furosemide distribution.[47] Permeability-limited liver model and mechanistic kidney model were used for prediction of furosemide disposition, which encompass metabolism mediated by UGT1A9 in liver and kidney, and active secretion into urine mediated by OATs, i.e., OAT1 and OAT3 in conjunction with MRP4. Based on literature reports,[24,25] fraction metabolized (f_m) by UGT1A9 was back calculated from observed total systemic clearance and renal clearance values,[24,25] using retrograde enzyme kinetics module of Simcyp. Although both OAT1 and OAT3 mediate the renal uptake of furosemide, due to missing literature data on the relative contribution of these transporters, we assumed that the secretion is entirely mediated by OAT3-dependent. OAT mediated active secretion was considered to be rate determining step for its renal uptake directly impacting furosemide plasma levels,[25,48,49] whereas MRP4 was assumed to regulate urine and tissue concentration, without impacting its plasma concentration.[50] Briefly, literature reported *in vitro* kinetic parameters of OAT3-mediated furosemide transport,[51] were incorporated and relative activity factor (RAF) was optimized to match the *in vivo* disposition (fe~65%).[24] MRP4 mediated active secretion into urine was also incorporated by using kinetic parameters generated in house using vesicular assay. The RAF for MRP4 mediated transport at apical side was optimized, so that the predicted cumulative urinary excretion-time profiles became consistent with observed cumulative urinary excretion-time profiles in clinical studies.[23,52] The disposition model was used to predict the PK of furosemide at

two different IV bolus doses i.e., 40 mg and 80 mg. The disposition model was also extrapolated to estimate the effect of disease state, i.e., liver cirrhosis on PK of furosemide. Simcyp liver cirrhosis (Child Pugh score A) model was used to predict changes in clearance of furosemide. For further verification of the disposition model, we also predicted the effect of OAT3 inhibitor-probenecid (parameters summarized in **Supplementary Table S5**) and compared against *in vivo* data.[25]

b. Development of oral PBPK model in adults

A multilayer- advanced dissolution absorption and metabolism (M-ADAM) model was used for furosemide absorption prediction. This model treats the gastro-intestinal tract as seven compartments and integrates absorption kinetics data along with *in vitro* experimental data, i.e., pH-dependent solubility profile,[28] human effective permeability (P_{eff}) that was calculated from Caco-2 permeability[31] and in house generated BCRP mediated efflux incorporated at apical side of intestinal epithelium. Further, to capture the rapid absorption phase, we incorporated apical uptake mediated by OATP2B1 along with MRP4 mediated efflux at basolateral side. The apical uptake clearance value was determined by sensitivity analysis and the clinical data, until the predicted plasma concentration-time profiles of furosemide administered in fasting state became consistent with observed data.[23,53] On the other hand, inter system extrapolation factor (ISEF) values for BCRP mediated apical efflux and MRP4 mediated basolateral efflux/exchange in intestinal epithelium were optimized by automated sensitivity analysis, or parameter estimation techniques until the predicted plasma- concentration profiles overlapped the observed data.[23] Once the plasma concentration profiles and PK parameters were captured adequately, the model was extrapolated to estimate the effect of food on PK of furosemide by using fed state physiology in Simcyp. Finally, a thorough sensitivity analysis was performed on furosemide oral

absorption model to investigate the impact of individual parameters, i.e., apical uptake $CL_{int,\ OATP2B1}$ (range of 0.02- 1 µl/min/mg), $ISEF_{BCRP}$ (10-200), and $ISEF_{MRP4}$ (10-100), and gastric emptying time (1-6 hr) to explore their potential impact on the bioavailability.

c. Model Evaluation:

To assess the robustness of the resulting PBPK model for furosemide, a visual comparison of the plasma concentration-time profiles observed in different clinical studies was done with those predicted by the model. The simulations were considered to be adequate when the observed data points were within the predicted 5th and 95th percentile and the simulated PK parameters were similar to observed clinical studies. Clinical data were digitized using Plot Digitizer (version 2.6.8).

2.7 Data analysis

For vesicular efflux assays, the net vesicular transport was calculated as the difference of Transport (ATP) – Transport (AMP). The kinetic parameters of vesicular transport were obtained by fitting the Michaelis-Menten equation $J = J_{max}\,[S]/([S] + K_m)$, where J is the velocity in pmol/min/mg protein, J_{max} is maximal velocity, [S] is substrate concentration (µM), and K_m is the Michaelis-Menten constant, using GraphPad Prism version 5.0 (La Jolla, CA). All the experiments were performed in triplicate and the results are expressed as mean and standard deviation. The transporter activity (pmol/min/pmol of transporter) was determined using previously reported values (**Supplementary Table S6**) of %inside-out vesicles using 5'-nucleotidase activity assay[39] and protein abundance in vesicles as described in Equation 1.

$$\text{Transporter activity}\left(\frac{\frac{\text{pmol}}{\text{min}}}{\text{pmol of transporter}}\right) = \frac{\text{Jmax, vesicles (pmol/min/mg)}}{(\text{Evesicles, total} * \%\text{inside out})} \qquad (1)$$

For cellular uptake assays, the transport facilitated by OATP2B1 was determined using Equation 2.

$$\text{Uptake}_{\text{OATP2B1}} = \text{Uptake}_{\text{MDCK-II, OATP2B1}} - \text{Uptake}_{\text{MDCK-II, MOCK}} \quad (2)$$

where $\text{Uptake}_{\text{MDCK-II, OATP2B1}}$ and $\text{Uptake}_{\text{MDCK-II, MOCK}}$ are uptake values (pmol/min/mg-protein) obtained in OATP2B1-transfected MDCK-II cells and mock-transfected MDCK-II cells, respectively.

3. RESULTS

ATP-dependent vesicular transport of furosemide

The initial ATP-dependent vesicular transport screening results confirmed BCRP and MRP4 as the main transporters involved in efflux of furosemide. P-gp, MRP2 and MRP3 expressing vesicles did not show any active transport of furosemide (**Supplementary Fig. 3**). The mean derived kinetic parameters, i.e., J_{max} and K_m from the kinetic curves (**Fig. 1**) were: 11307 pmol/min/mg and 20.9 µM (BCRP) and 554.2 pmol/min/mg and 27.96 µM (MRP4), respectively (**Table 2**).

Time- and concentration-dependent uptake of furosemide in hOATP2B1 transfected cells

The uptake of furosemide by OATP2B1-transfected cells was >2-fold higher than the uptake by mock cells at 15 min (**Fig. 2A**). Using 15 min incubation time, the OATP2B1-mediated uptake was linear up to 500 µM (**Fig. 2B)**. Kinetics parameters of OATP2B1 mediated uptake of furosemide could not be derived as saturation of the uptake rate was not achieved due to poor solubility of furosemide at concentration >500 µM.

Protein abundance of efflux and uptake transporters

The protein abundances of BCRP and MRP4 in vesicles were 11.4 and 0.3 pmol/mg protein, respectively. As P-gp, MRP2, and MRP3 did not transport furosemide in the initial screening, their protein abundance values are not shown. The % of inside-out vesicles was observed to be 33% (BCRP) and 21% (MRP4). The protein abundance of OATP2B1 in the transfected MDCK-II cells was 4.25 pmol/mg protein (**Supplementary Table S6**).

Furosemide PBPK IV model development and validation

The RAF values of 65.49 and 70.3 were obtained for OAT3 and MRP4 mediated disposition, by optimization using parameter estimation module and the clinical data.[21,23,25,44,46] UGT1A9-mediated clearance of 42 µl/min/mg was back calculated by subtracting OAT3 mediated clearance from total systemic clearance.[24,25] The model adequately predicted furosemide PK at two IV bolus doses, i.e., 40 mg and 80 mg (**Fig. 3)**, where all the observed data points were within 95th and 5th percentile of all simulations. The cumulative urinary excretion-time profiles of respective IV doses were in accordance with the observed data (**Supplementary Fig. 4**)[23,52]. Corresponding predicted versus observed PK parameters are shown in **Table 3**, which further confirm that furosemide disposition was well captured by the model. Final model simulated percent contributions of metabolism and excretion, i.e., f_m of~35% and f_e of~65% were in accordance with literature values.[24,25] The developed model was then used to successfully predict the effect of i) liver cirrhosis for 80 mg IV bolus dose (**Fig. 4**)[45] and ii) OAT3 inhibitor, probenecid on furosemide PK (**Fig. 5**).[25]

Furosemide PBPK oral model development and validation

In oral model, the apical uptake and efflux of furosemide mediated by OATP2B1 and BCRP and basolateral efflux mediated by MRP4, were incorporated into the model to reflect the *in vitro* findings that furosemide absorption is governed by combination of uptake and efflux mechanisms. The reported low permeability value was unable to capture oral absorption profile (**Supplementary Fig. 5**). Incorporating apical uptake clearance ($CL_{int,\ OATP2B1}$) along with MRP4 mediated basolateral efflux, obtained by parameter sensitivity analysis were able to capture *in vivo* absorption (**Fig. 6**).[23] ISEF values obtained for BCRP mediated apical efflux and MRP4 mediated basolateral efflux were 100 and 25, respectively. Our model was also able to capture the food-effect as shown in (**Fig. 4**). The sensitivity analysis of individual parameters, i.e., apical uptake $CL_{int,\ OATP2B1}$ (range of 0.02- 1 µl/min/mg), $ISEF_{BCRP}$ (10-200), and $ISEF_{MRP4}$ (10-100), and gastric emptying time (1-6 hr) are shown in **Fig. 7**. The sensitivity analysis for apical uptake CL revealed that when values were low, the Cmax and AUC were lower whereas converse is true for apical efflux clearance. Interplay of uptake and efflux transporters at differential rates would play a significant role in governing furosemide transport across gastro-intestinal epithelium as demonstrated by sensitivity analysis, thereby impacting overall bioavailability.

4. DISCUSSION

Oral absorption of furosemide is highly variable which differs markedly across different dosage forms or formulations (solution vs. tablet or immediate vs. sustained release formulation), with or without food, and between healthy vs. disease state.[2] Furosemide is a BCS class IV drug; its poor solubility and permeability are considered to be the determinants of its variable bioavailability.[54] Furosemide is a weak acid and exhibits pH-dependent solubility, and the

dissolution studies predict that furosemide solubility is ~20-fold higher in fed-state simulated gastric fluid as compared to fasted-state simulated gastric fluid.[36] However, the higher solubility in fed-state dissolution media does not correlate with furosemide oral absorption as majority of the food-effect studies report reduced bioavailability.[23,34,35] This indicates that furosemide absorption is not solubility-limited, a phenomenon supported by the shorter mean dissolution time (MDT) in comparison to the mean absorption time (MAT) established by moment analysis of clinical data.[23] Moreover, the reported MAT of oral solution is significantly longer than the mean residence time (MRT) after IV bolus dose, indicating flip-flop and absorption-rate limited kinetics.[23] Using moment analysis of clinical data, it is previously[23] suggested that furosemide absorption is limited by transport across gastro-intestinal epithelium or gastric emptying.

To mechanistically explain furosemide clinical PK data, we investigated role of intestinal transporters in furosemide absorption. We identified that BCRP and MRP4 are the major efflux transporters and OATP2B1 is the key uptake transporter governing furosemide absorption at apical and basolateral side of gastro-intestinal epithelium. Modulation of these transport mechanisms by drug-interactions or genetic polymorphisms could play a substantial role in limiting furosemide absorption. Our data showed that furosemide is not a substrate of P-gp consistent with Flanagan et al. data.[55] However, the latter contradicts with another report which showed an efficient inhibition of furosemide transport by verapamil (200 µg/ml) in exercised rat jejunum experiment.[33] Considering the latter study used high verapamil concentration, it can be postulated that the effect observed was a result of non-selective inhibition of other efflux transporters. Similar to our findings, Flanagan et al. confirmed that MRP1 and MRP2 are not involved in the secretion of furosemide.[55]

Although furosemide was previously shown to be a substrate of BCRP and MRP4 using in vitro and in vivo models,[50] our study characterized, for the first time, the kinetic parameters of BCRP and MRP4 mediate uptake in membrane vesicles, which were further integrated into a mechanistic PBPK model to explain the variable absorption of furosemide. Furosemide is a substrate of OATP2B1 that works in tandem with MRP4 in the enterocytes, both of which facilitate its rapid absorption. These results explain moderate to high oral bioavailability,[23,56,57] which otherwise cannot be predicted using its low passive permeability data.[30,31] Unlike previously established role of hepatic OATPs (OATP1B1 and OATP1B3) in furosemide uptake,[31] contribution of intestinal OATP in furosemide absorption is a novel finding of our study. While there are no reported PK studies where furosemide was co-administered with known OATP2B1 inhibitors, OATP1B inhibitors such as aliskiren, lesinurad, valsartan, and sacubitril significantly reduce furosemide absorption.[58–60] Because OATP1B1 and OATP1B3 are not expressed in the intestine, this effect is perhaps due to OATP2B1 inhibition, which can be confirmed in future studies. As fruit juices such as grapefruit, apple and orange juices are known to modulate OATP2B1 activity, this could be another plausible reason for variable absorption and food effect.

The extent of absorption is influenced by presence or absence of food. Although, food increases the stomach pH and facilitate lipid-mediated solubilization, these factors do not explain negative food effect observed in case of furosemide. On the other hand, delayed gastric emptying can change the luminal concentrations that can influence saturation kinetics of efflux transporter/intestinal metabolism. For example, the predicted luminal concentrations of furosemide in fasting conditions are higher than the Km value of 20.9 µM for BCRP. The latter suggests that the high luminal concentrations in fasting condition could saturate BCRP. On the

other hand, in fed condition, delayed gastric emptying results in lower luminal concentrations, which would be insufficient to saturate BCRP, thus resulting in efficient BCRP-mediated efflux. Hence, reduction in bioavailability of furosemide might be a consequence of efficient BCRP efflux as a result of delayed gastric emptying. This hypothesis could be further confirmed by conducting food effect studies in BCRP knockout models or in presence of BCRP inhibitors as reported previously.[61] Sensitivity analysis of individual parameters revealed that all the transporters could differentially impact bioavailability, however changes in apical uptake, apical efflux, and gastric emptying would have high influence on initial rate of absorption whereas all four parameters can impact overall extent of absorption.

Role of MRP4 in furosemide uptake is not only limited to oral absorption but can also be applied to other organs such as kidney in conjunction with uptake transporters. For example, furosemide is a known potent substrate of OAT1/3 expressed in basolateral membrane of kidney proximal tubule which work in concert with MRP4 at the apical side. Thus, MRP4 could play a crucial role in regulating furosemide concentration in the proximal tubules, the site of action.[62] This corroborates with the fact that the therapeutic response of furosemide is related to drug concentration in urine,[63] as opposed to that in plasma and the diuretic activity is effectively blocked by OAT1/3 inhibitor, probenecid.[48] This implies that diuretic activity of furosemide can be influenced by both OAT and MRP4 function in a synergistic manner. Further, MRP4 genetic polymorphism (g.33387C > A) has been shown to be associated with weight loss when furosemide is given in decompensated heart failure patients,[64] indicating that altered MRP4 function due to drug interactions, aging, and pathophysiological factors can cause secondary effects of furosemide.

With the emerging regulatory significance of renal transporters, furosemide has been proposed as a probe substrate of renal OATs for assessing clinical DDIs during drug development. Particularly, furosemide was used in recent cocktail in vivo transport studies.[65,66] As furosemide is identified as a substrate for BCRP, MRP4 and OATP2B1 in this study, confounding effects of these transporters on furosemide PK should be considered while interpreting such clinical DDI studies.

FIGURES

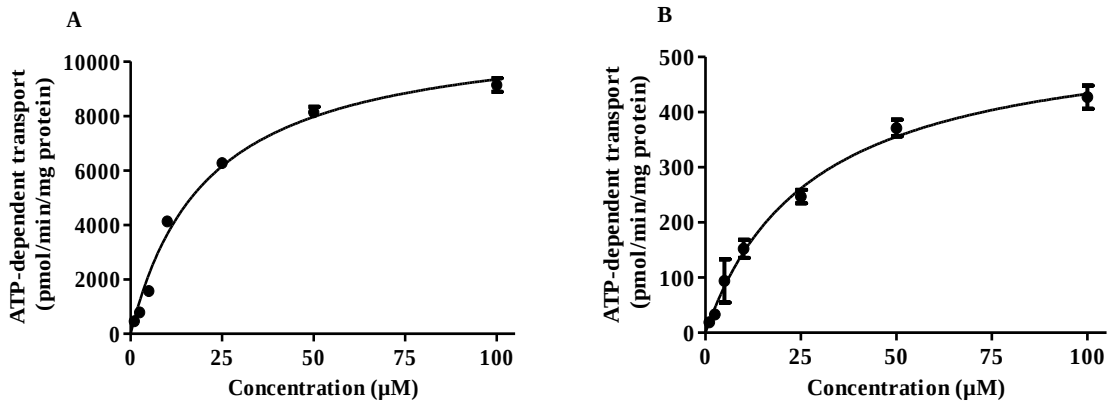

Fig. 1. ATP-dependent transport kinetics of furosemide in BCRP (A) and MRP4 (B) vesicles. The kinetic experiments were conducted at various concentrations (i.e., 1 to 100 µM) with 25 µg vesicle proteins for 30 seconds. Differences between the ATP and AMP groups (net ATP-dependent transport rates) were calculated and Michaelis-Menten equation (J = Jmax*[S]/([S]+Km)) was fitted to the data and represented as the mean (SD (n = 3)). The kinetic constants (Jmax and Km with the 95% CI) for the studied efflux transporters are presented in **Table 1**.

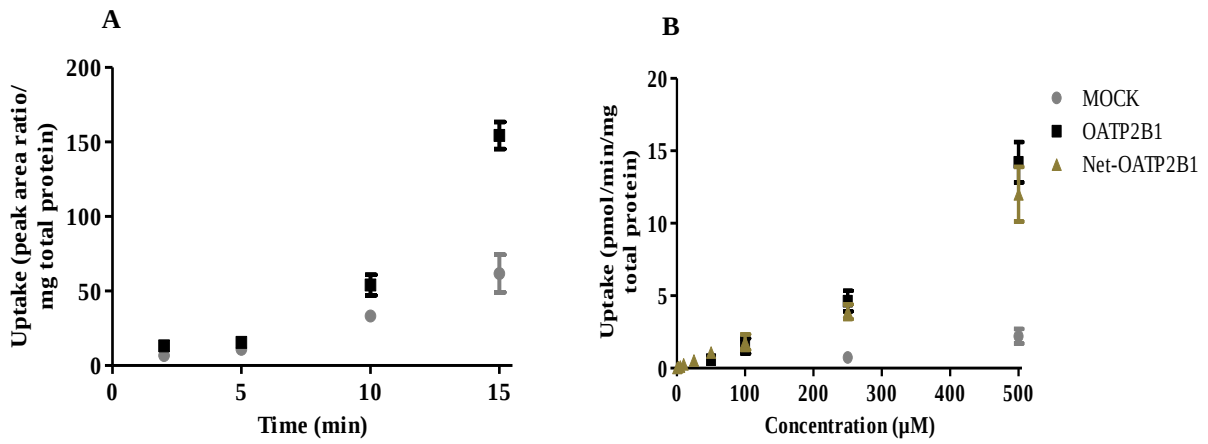

Fig. 2. Time- and concentration-dependent OATP2B1-mediated uptake of furosemide by mock and OATP2B1 transfected MDCK-II cells. Uptake was measured at 37 ºC over specified time (i.e., 2, 5, 10 and 15 min, as shown in A) and in the concentration range (i.e., 0.5 to 500 µm for 15 min, as shown in B). The OATP2B1-specific rate of uptake in concentration dependent studies, was obtained by subtracting the uptake in mock cells from that of OATP2B1-transfected MDCK-II cells. The OATP2B1-specific rate was linear in the measured concentration range. Each data point represents the mean ± SD (n = 3).

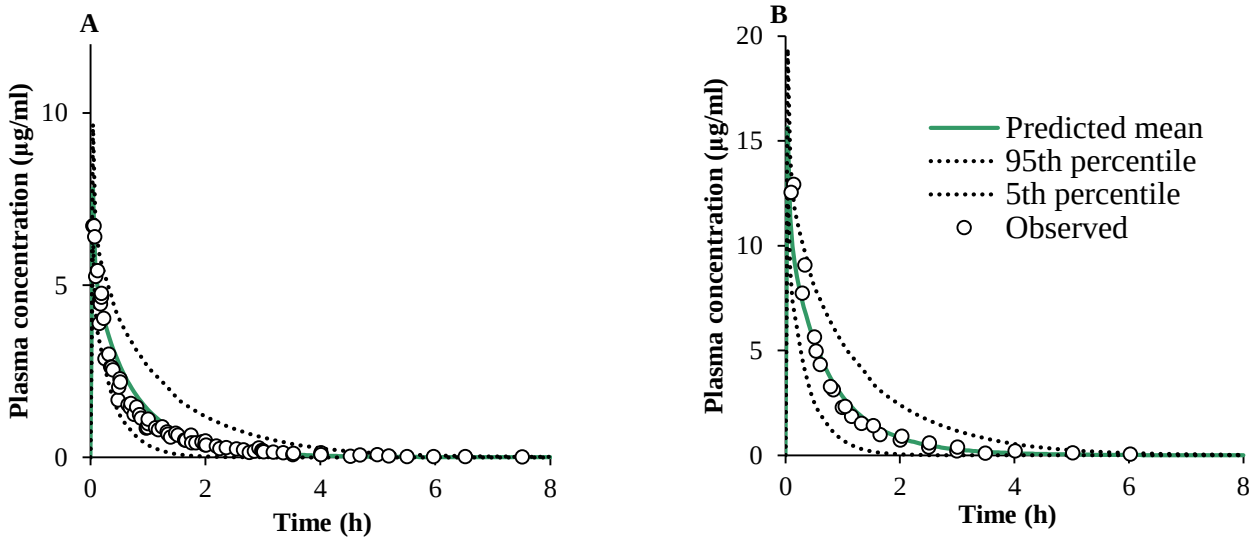

Fig. 3. PBPK model-simulated concentration–time profiles for furosemide given intravenously at doses 40 mg (A) and 80 mg (B) in healthy volunteers. Included in each plot is the predicted mean, 95th percentile and 5th percentile concentration range. The open circles represent mean observed data reported.[21,23,25,44–46]

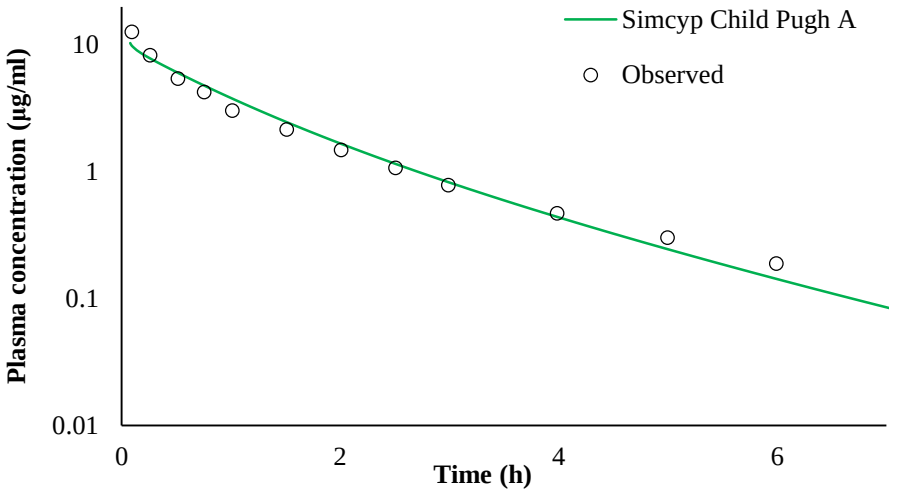

Fig. 4. PBPK model-simulated furosemide plasma concentration–time profiles in subjects with cirrhotic subjects. The continuous green (solid) line is the predicted profile using the default Simcyp Child Pugh A model. The open circles represent mean observed data reported.[45]

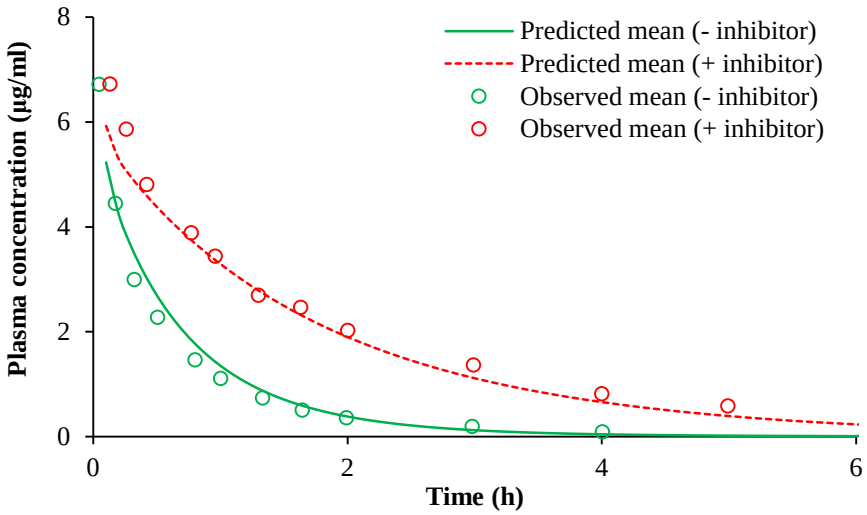

Fig. 5. PBPK model-simulated concentration–time profiles of furosemide given intravenously at dose 40 mg along with probenecid (OAT1/3 inhibitor). The continuous green (solid) line is the predicted profile of furosemide given a single dose of 40 mg intravenously in absence of OAT1/3 inhibitor and the red (dashed) line is the predicted profile of furosemide given as a single dose of 40 mg intravenously along with OAT1/3 inhibitor i.e., probenecid administered as doses of 1000 mg twice orally (i.e., 13 hours and 1 hour) before furosemide administration. The open circles represent mean observed data reported.[25]

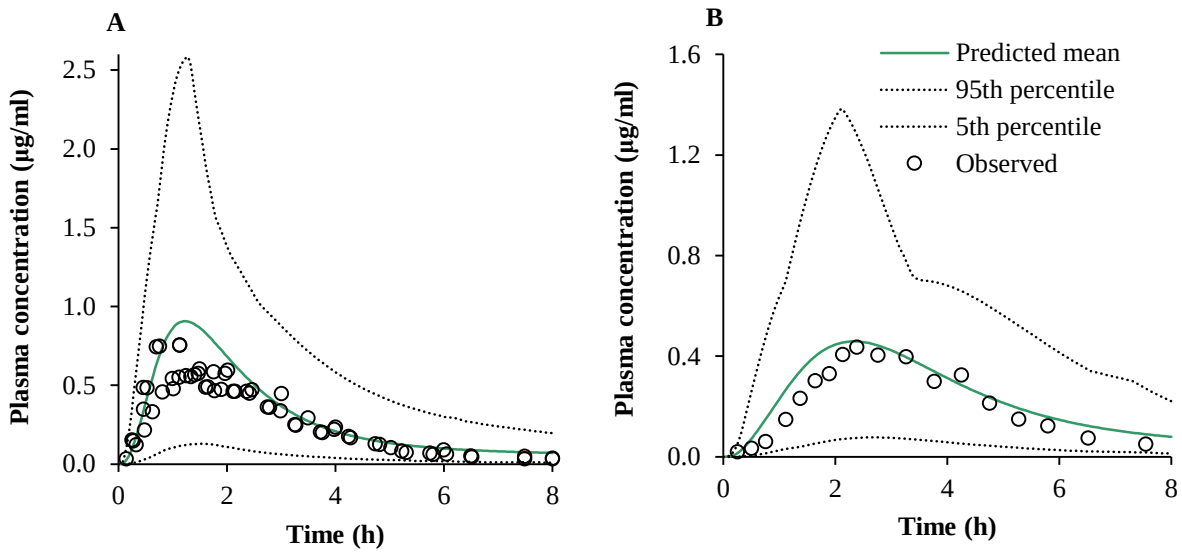

Fig. 6. PBPK model-simulated concentration–time profiles for furosemide given orally at dose 40 mg in fasting (A) and fed (B) conditions in healthy volunteers. Included in each plot is the predicted mean, 95th percentile and 5th percentile concentration range. The open circles represent mean observed data reported.[23,53]

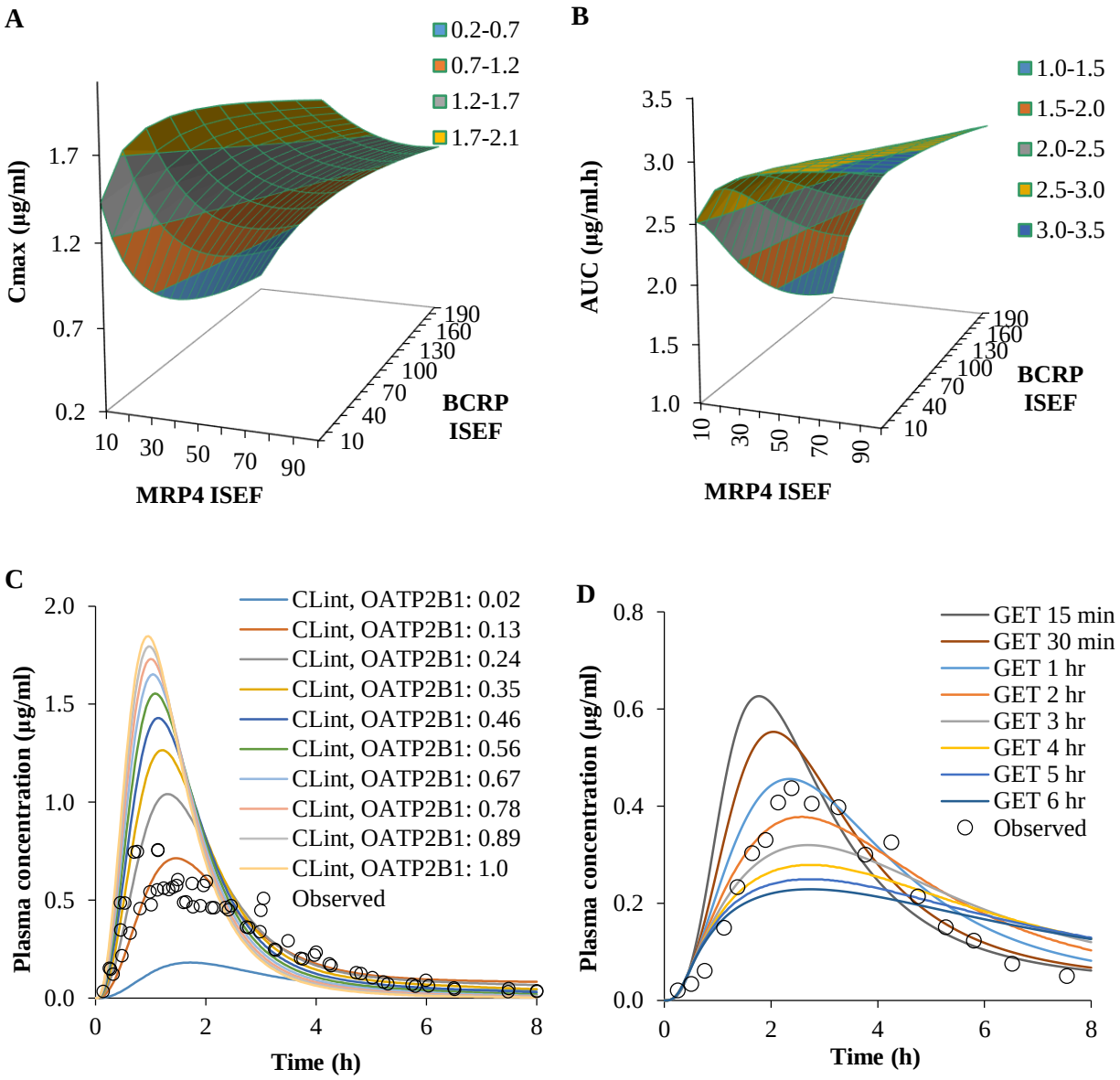

Fig. 7. Sensitivity analysis of the developed mechanistic-oral absorption model. The sensitivity analysis of individual parameters i.e., $ISEF_{BCRP}$ (10-200), and $ISEF_{MRP4}$ (10-100) to evaluate their effects on simulated rate (C_{max}) and extent of absorption (AUC) and are shown in panel A and B. We also conducted sensitivity analysis of apical uptake $CL_{int,\ OATP2B1}$ (range of 0.02- 1 µl/min/mg) in fasting condition and gastric emptying time (1-6 hr) in fed condition, to evaluate their effects on initial rate of absorption, data shown in panel C and D. The open circles represent mean observed data reported.[23,53]

SUPPLEMENTARY FIGURES

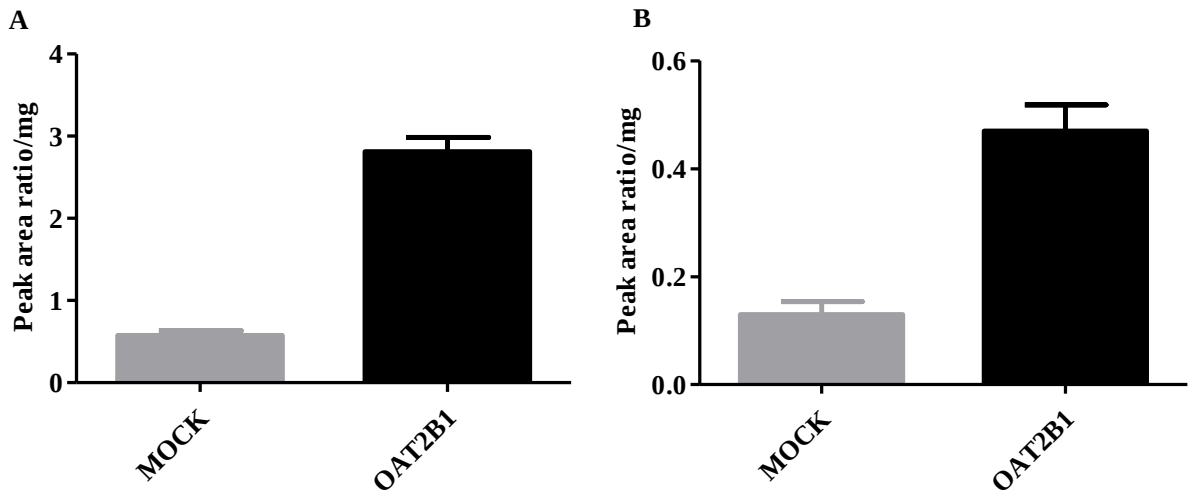

Supplementary Fig. 1. Uptake of OATP2B1 probe substrates i.e., estrone-3-sulfate (A) and rosuvastatin (B) in mock and hOATP2B1-transfected MDCK-II cells at 2 µM substrate concentration. Each data point represents the mean ± SD (n = 3). The functional transport activity of hOATP2B1-transfected cells was confirmed by significant difference (~ 4 to 5 fold) between hOATP2B1-transfected and mock-transfected cells.

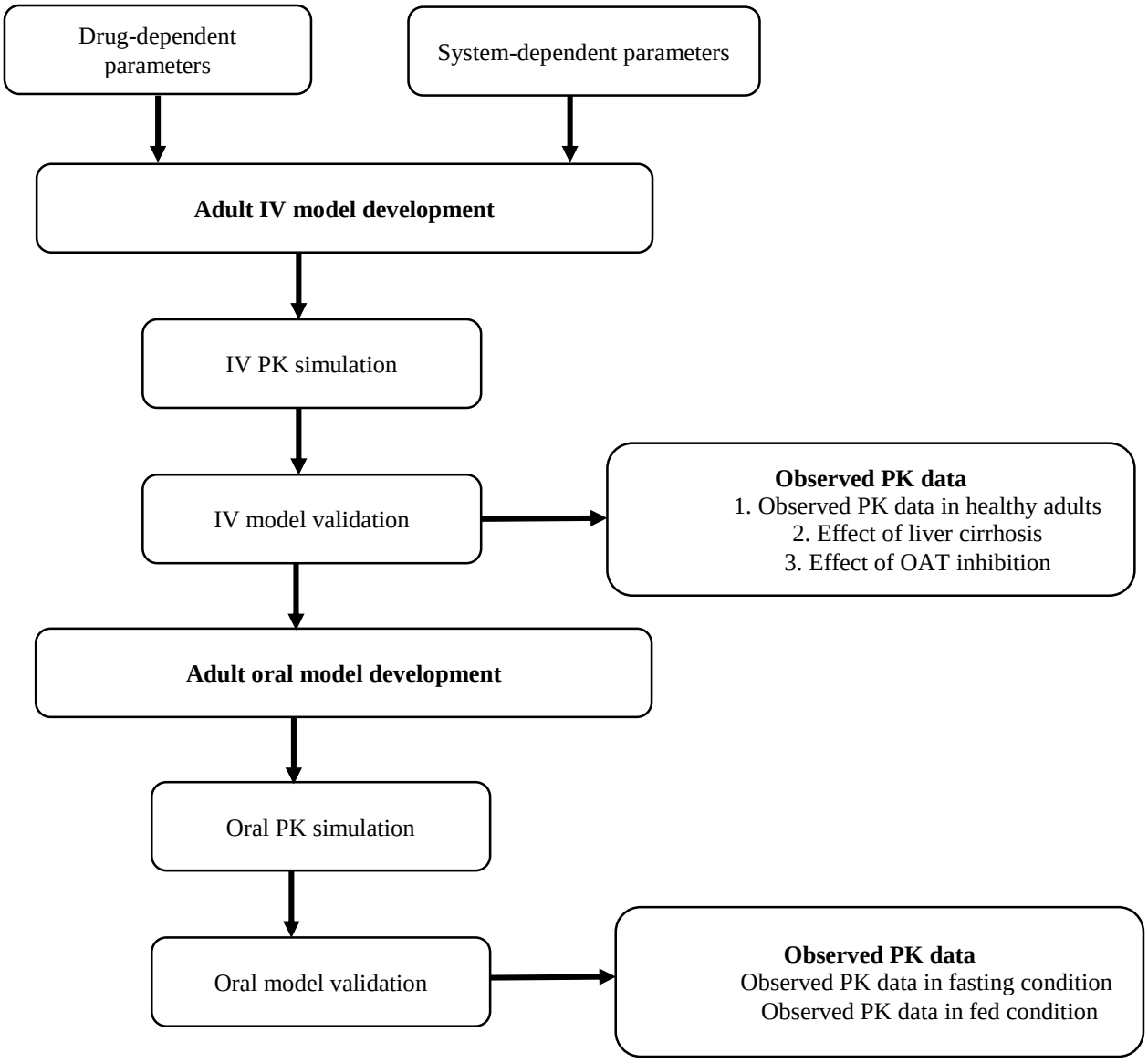

Supplementary Fig. 2. Schematic diagram of furosemide PBPK model development and validation.

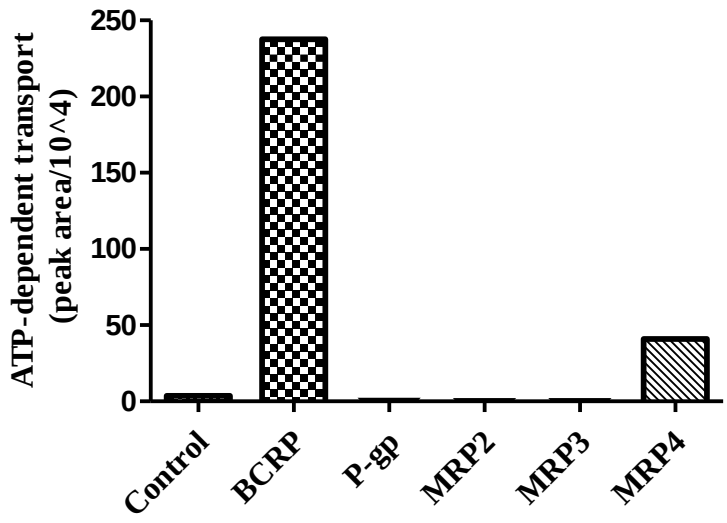

Supplementary Fig. 3. Screening of ATP-dependent transport rate of furosemide in membrane vesicles overexpressing efflux transporters at 10 µM substrate concentration. The transport of furosemide by BCRP, P-gp, MRP2, MRP3, and MRP4 was studied using 25 µg of total vesicle protein and 1 min incubation. Control vesicles (Ctrl) prepared using HEK293 cells expressing empty vector (mock) were used in all assays. Net ATP-dependent transport was calculated as difference between the ATP and AMP. Furosemide was not found to be a substrate of P-gp, MRP2 and MRP3.

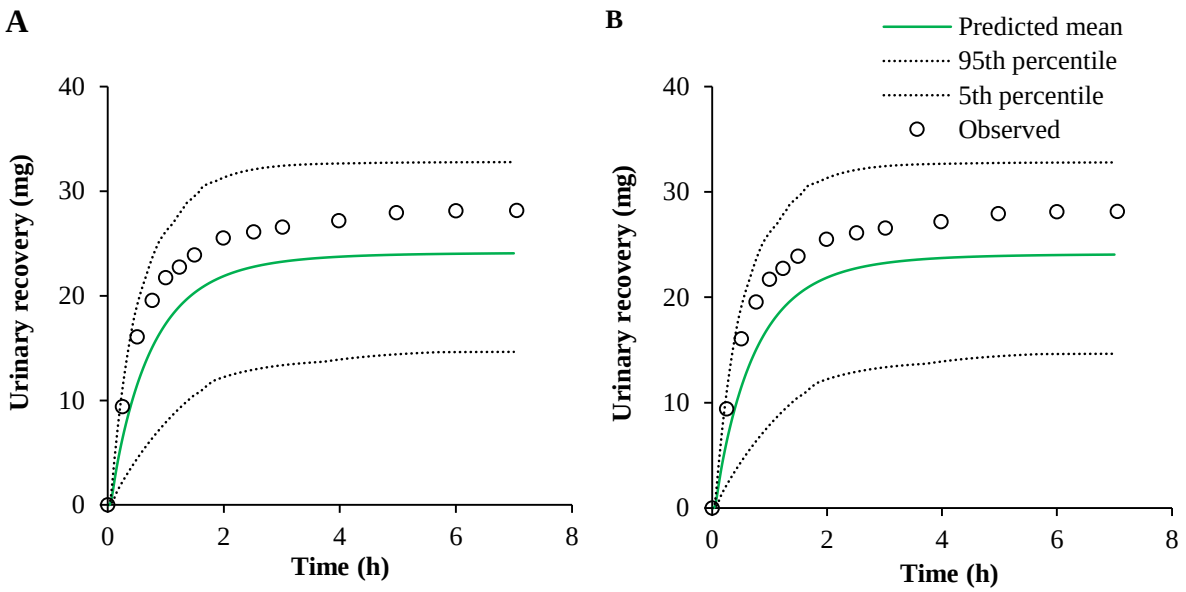

Supplementary Fig. 4. PBPK model-simulated profiles of furosemide excreted in urine over time range when given intravenously at doses 40 mg (A) and 80 mg (B) in healthy volunteers. Included in each plot is the predicted mean, 95th percentile and 5th percentile concentration range. The open circles represent mean observed data reported.[23,52]

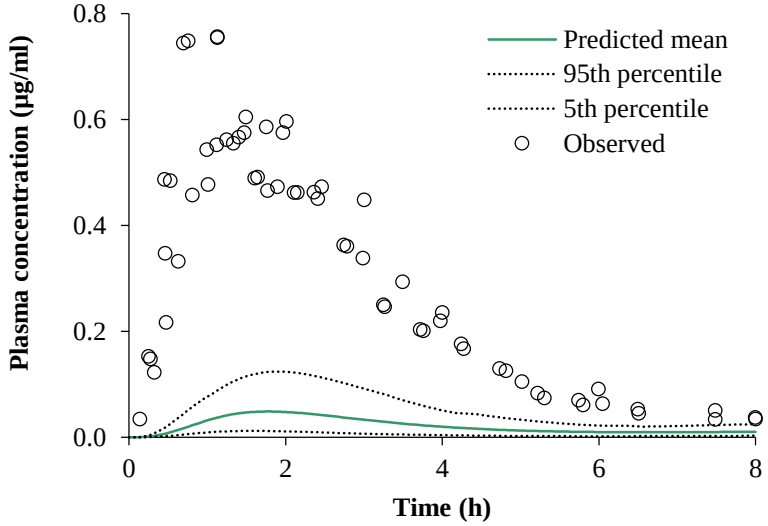

Supplementary Fig. 5. PBPK model-simulated profiles of furosemide given orally at dose 40 mg in fasting condition in healthy volunteers using $P_{app} \leq 2.0 \times 10^{-6}$ cm/sec. Included in each plot is the predicted mean, 95th percentile and 5th percentile concentration range. The open circles represent mean observed data reported.[23,53] The low permeability value failed to capture the observed oral absorption profile.

TABLES

Table 1: Input parameters used for furosemide PBPK model development

PBPK parameter	Value	Method/reference(s)
1. Physico-chemical and binding		
Molecular mass (g/mol)	330.74	PUBCHEM database
LogP	2.29	PUBCHEM database
pKa	3.9	PUBCHEM database
B/P ratio	0.6	Reported[42]
fu, plasma	0.03	Reported[37,43]
2. Absorption		
Model	M-ADAM	
$P_{eff,\ human}$ (*10^{-4} cm/s)	0.39	Estimated[a]
Apical uptake (intestine)		
$CL_{int,\ OATP2B1}$ (µl/min/10^6 cells)	0.2	Optimized[b]
Apical efflux (intestine)		
$J_{max,\ BCRP}$ (pmol/min/pmol)	3037	Experimental
K_m(µM)	20.9	Experimental
ISEF	100	Optimized[b]
Basolateral efflux (intestine)		
$J_{max,\ MRP4}$ (pmol/min/pmol)	9085.2	Experimental
K_m(µM)	27.96	Experimental
ISEF	25	Optimized[b]
3. Distribution		
Model	Full PBPK	
Vss (L/kg)	0.1	Method 2[47]
4. Elimination		
$CL_{int,\ UGT1A9}$ (µl/min/mg protein)	42	Estimated[c]
Permeability limited liver model		
Sinusoidal active uptake $CL_{int,\ T}$ (µl/min/10^6cells)	9	Optimized[b]
Permeability limited kidney model		
$J_{max,\ OAT3\ (basolateral)}$ (pmol/min/10^6cells)	54.17	Reported[51]
K_m(µM)	12.95	Reported[51]
RAF	65.5	Optimized[a]
$J_{max,\ MRP4\ (apical)}$ (pmol/min/10^6cells)	118.23	Experimental
K_m (µM)	27.96	Experimental
RAF	70.3	Optimized[a]

[1]Estimated based on experimental caco-2 permeability.[31]

[2]Optimization involves manual or automated sensitivity analysis, or parameter estimation techniques, where the predicted plasma- concentration and/or urinary excretion profiles overlapped the observed data.[21,23,25,44–46]

[3]Estimated by back calculation from *in vivo* systemic and renal clearance,[25] using retrograde enzyme kinetics in simcyp to match in vivo fraction metabolized (i.e., fm~35%).[24]

Experimental: *in vitro* experimental value generated in house using overexpressing membrane vesicles.

Table 2: Kinetic parameters (K_m and J_{max}) for the transport of furosemide derived using BCRP and MRP4 overexpressing vesicles after fitting the Michaelis-Menten equations. Values in parentheses represent 95% confidence intervals (CI).

Transporter	**K_m, µM (95% CI)**	**J_{max}, pmol/min/mg (95% CI)**	**Normalized average J_{max} (pmol/min/pmol of transporter protein)**
BCRP	20.9 (16.4 to 25.3)	11296 (10437 to 12155)	3037
MRP4	27.96 (19.5 to 36.5)	554.2 (489.1 to 619.3)	9085.2

Table 3: Model validation: Comparison of predicted and observed PK data of furosemide in adults

A. Intravenous (IV) bolus formulation (healthy subjects)

	Dose 40 mg		Dose 80 mg	
	Observed[a]	Predicted[b]	Observed[a]	Predicted[b]
Cmax (μg/ml)	6.7, 6.4	7.8	12.5, 12.9	15.6
AUC (μg/ml*hr)	4.1, 4.2	4.2	9.3, 9.2	8.5

[a]Parameter estimates obtained from references. [21,23,25,44–46]

[b]Estimates based on PBPK model simulations using the Simcyp simulator

B. Intravenous (IV) bolus formulation (liver cirrhotic patients)

IV dose 80 mg	Observed[a]	Predicted[b]
Cmax (μg/ml)	12.7	13.5
AUC (μg/ml*hr)	11.9	11.5

[a]Parameter estimates obtained from references.[45]

C. Intravenous (IV) bolus formulation (healthy subjects with OAT3 inhibitor, probenecid)

IV dose 40 mg	Without inhibitor		With inhibitor	
	Observed[a]	Predicted[b]	Observed[a]	Predicted[b]
C_{max} (μg/ml)	6.4	7.8	6.7	5.9
AUC (μg/ml*hr)	4.2	4.2	12.3	10.1

[a]Parameter estimates obtained from references.[25]

D. Oral tablet (healthy subjects)

PO dose 40 mg	Fasting condition		Fed condition	
	Observed[a]	Predicted[b]	Observed[a]	Predicted[b]
Cmax (μg/ml)	0.6 ± 0.3	0.43	0.43	0.46
AUC (μg/ml*hr)	2.1 ± 1.1	1.83	1.83	1.92

[a]Parameter estimates obtained from references.[23,53]

SUPPLEMENTARY TABLES

Supplementary Table S1: Transport activity of selected probe substrates by individual transporter in vesicular transport assay.

Transporter	Compound	Final concentration (mM)	Incubation time (min)	Transport rate (pmol/mg/min)	SD
Control	E217bG	100	5	0.31	
MRP2	E217bG			4427.34	221.04
Control	E217bG	10	10	4.08	1.71
MRP3	E217bG			385.95	22.28
Control	NMQ	2	1	---	---
P-gp	NMQ			1981.61	206.45
Control	DHEAS	0.5	1.5	1.15	0.27
MRP4	DHEAS			97.94	12.66
Control	E3S	1	1	3.98	2.06
BCRP	E3S			448.45	46.71

Estradiol-17β-glucuronide (E2-17β-G)

N-Methyl Quinidine (NMQ)

dehydroepiandrosterone sulfate (DHEAS)

estrone-3-sulfate (E3S)

Supplementary Table S2: LC conditions for transporter surrogate peptide quantification.

Column	UPLC column (Acquity UPLC HSS T3 1.8 µm, 2.1 x 100 mm, Waters			
Guard column	Security Guard column (C18, 4 mm x 2.0 mm, Phenomenex)			
Run Time	27.00 min			
Injection volume	5 µl			
Column oven temperature	25 °C			
Autosampler temperature	6 °C			
Gradient Table:				
Time	Flow Rate	%A	%B	Curve
Initial	0.300	97.0	3.0	Initial
4.00	0.300	97.0	3.0	6
8.00	0.300	87.0	13.0	6
18.00	0.300	70.0	30.0	6
20.50	0.300	65.0	35.0	6
21.10	0.300	40.0	60.0	6
23.10	0.300	20.0	80.0	6
23.20	0.300	97.0	3.0	6
27.00	0.300	97.0	3.0	6
A = 0.1% formic acid water; B = 0.1% formic acid acetonitrile				

Supplementary Table S3: Surrogate peptides of efflux transporters and their MS/MS parameters.

Protein name	Surrogate peptide	Peptide type	Parent Ion	Fragment Ion	Cone Voltage	Collision energy	On-column calibration range (fmol)
BCRP	SSLLDVLAAR	light	522.806	757.457	69.2	27.7	0.12 to 59.87
BCRP	SSLLDVLAAR	light	522.806	644.373	69.2	27.7	
BCRP	SSLLDVLAAR	light	522.806	529.346	69.2	27.7	
BCRP	SSLLDVLAAR	heavy	527.81	767.465	69.2	27.7	
BCRP	SSLLDVLAAR	heavy	527.81	654.381	69.2	27.7	
BCRP	SSLLDVLAAR	heavy	527.81	539.354	69.2	27.7	
BCRP	VIQELGLDK	light	507.795	802.43	68.1	27.1	
BCRP	VIQELGLDK	light	507.795	674.372	68.1	27.1	
BCRP	VIQELGLDK	light	507.795	545.329	68.1	27.1	
BCRP	VIQELGLDK	heavy	511.802	810.445	68.1	27.1	
BCRP	VIQELGLDK	heavy	511.802	682.386	68.1	27.1	
BCRP	VIQELGLDK	heavy	511.802	553.344	68.1	27.1	
P-gp	EIIGVVSQEPVLFATTIAENIR	light	800.444	917.505	89.5	41.1	
P-gp	EIIGVVSQEPVLFATTIAENIR	light	800.444	715.41	89.5	41.1	
P-gp	EIIGVVSQEPVLFATTIAENIR	light	800.444	602.326	89.5	41.1	
P-gp	EIIGVVSQEPVLFATTIAENIR	heavy	803.78	927.513	89.5	41.1	
P-gp	EIIGVVSQEPVLFATTIAENIR	heavy	803.78	725.418	89.5	41.1	
P-gp	EIIGVVSQEPVLFATTIAENIR	heavy	803.78	612.334	89.5	41.1	
P-gp	IATEAIENFR	light	582.306	979.484	73.6	29.8	0.42 to 6.72
P-gp	IATEAIENFR	light	582.306	749.394	73.6	29.8	
P-gp	IATEAIENFR	light	582.306	565.273	73.6	29.8	
P-gp	IATEAIENFR	heavy	587.311	989.493	73.6	29.8	
P-gp	IATEAIENFR	heavy	587.311	759.402	73.6	29.8	
P-gp	IATEAIENFR	heavy	587.311	575.281	73.6	29.8	
P-gp	NTTGALTTR	light	467.751	719.405	65.2	25.7	0.42 to 13.38
P-gp	NTTGALTTR	light	467.751	618.357	65.2	25.7	
P-gp	NTTGALTTR	light	467.751	377.214	65.2	25.7	
P-gp	NTTGALTTR	heavy	472.755	729.413	65.2	25.7	
P-gp	NTTGALTTR	heavy	472.755	628.365	65.2	25.7	

P-gp	NTTGALTTR	heavy	472.755	387.223	65.2	25.7	
MRP2	LTIIPQDPILFSGSLR	light	590.677	1329.716	74.2	29.7	0.07 to 35.31
MRP2	LTIIPQDPILFSGSLR	light	590.677	779.441	74.2	29.7	
MRP2	LTIIPQDPILFSGSLR	light	590.677	666.357	74.2	29.7	
MRP2	LTIIPQDPILFSGSLR	light	590.677	665.362	74.2	29.7	
MRP2	LTIIPQDPILFSGSLR	heavy	594.013	1339.724	74.2	29.7	
MRP2	LTIIPQDPILFSGSLR	heavy	594.013	789.449	74.2	29.7	
MRP2	LTIIPQDPILFSGSLR	heavy	594.013	676.365	74.2	29.7	
MRP2	LTIIPQDPILFSGSLR	heavy	594.013	670.366	74.2	29.7	
MRP2	QLLNNILR	light	492.303	742.457	67	26.6	
MRP2	QLLNNILR	light	492.303	629.373	67	26.6	
MRP2	QLLNNILR	heavy	497.308	752.465	67	26.6	
MRP2	QLLNNILR	heavy	497.308	639.381	67	26.6	
MRP3	SQLTIIPQDPILFSGTLR	light	1000.065	1456.816	104	44.9	
MRP3	SQLTIIPQDPILFSGTLR	light	1000.065	1343.732	104	44.9	
MRP3	SQLTIIPQDPILFSGTLR	light	1000.065	1003.594	104	44.9	
MRP3	SQLTIIPQDPILFSGTLR	heavy	1005.069	1466.824	104	44.9	
MRP3	SQLTIIPQDPILFSGTLR	heavy	1005.069	1353.74	104	44.9	
MRP3	SQLTIIPQDPILFSGTLR	heavy	1005.069	1013.602	104	44.9	
MRP3	ADGALTQEEK	light	531.259	875.45	80	26	0.32 to 164.5
MRP3	ADGALTQEEK	light	531.259	747.39	80	26	
MRP3	ADGALTQEEK	light	531.259	634.3	80	26	
MRP3	ADGALTQEEK	heavy	535.266	883.46	80	26	
MRP3	ADGALTQEEK	heavy	535.266	755.4	80	26	
MRP3	ADGALTQEEK	heavy	535.266	642.32	80	26	
MRP4	AEAAALTETAK	light	538.285	875.483	70.4	28.2	
MRP4	AEAAALTETAK	light	538.285	733.409	70.4	28.2	
MRP4	AEAAALTETAK	light	538.285	662.372	70.4	28.2	
MRP4	AEAAALTETAK	heavy	542.292	883.497	70.4	28.2	
MRP4	AEAAALTETAK	heavy	542.292	741.423	70.4	28.2	
MRP4	AEAAALTETAK	heavy	542.292	670.386	70.4	28.2	
MRP4	LNTIIDSDK	light	509.774	905.457	68.3	27.2	
MRP4	LNTIIDSDK	light	509.774	453.232	68.3	27.2	
MRP4	LNTIIDSDK	light	509.774	396.211	68.3	27.2	
MRP4	LNTIIDSDK	light	509.774	888.431	68.3	27.2	

MRP4	LNTIIDSDK	light	509.774	302.135	68.3	27.2	
MRP4	LNTIIDSDK	heavy	513.781	913.472	68.3	27.2	
MRP4	LNTIIDSDK	heavy	513.781	457.239	68.3	27.2	
MRP4	LNTIIDSDK	heavy	513.781	400.218	68.3	27.2	
MRP4	LNTIIDSDK	heavy	513.781	896.445	68.3	27.2	
MRP4	TTTGQIVNLLSNDVNK	light	572.976	589.294	72.9	28.8	
MRP4	TTTGQIVNLLSNDVNK	light	572.976	395.209	72.9	28.8	
MRP4	TTTGQIVNLLSNDVNK	light	572.976	815.389	72.9	28.8	
MRP4	TTTGQIVNLLSNDVNK	light	572.976	702.305	72.9	28.8	
MRP4	TTTGQIVNLLSNDVNK	light	572.976	720.378	72.9	28.8	0.34 to 174.8
MRP4	TTTGQIVNLLSNDVNK	heavy	575.647	597.308	72.9	28.8	
MRP4	TTTGQIVNLLSNDVNK	heavy	575.647	399.216	72.9	28.8	
MRP4	TTTGQIVNLLSNDVNK	heavy	575.647	823.404	72.9	28.8	
MRP4	TTTGQIVNLLSNDVNK	heavy	575.647	710.32	72.9	28.8	
MRP4	TTTGQIVNLLSNDVNK	heavy	575.647	724.385	72.9	28.8	
MRP4	AASQILILK	light	478.811	260.197	66	26.1	
MRP4	AASQILILK	light	478.811	364.257	66	26.1	
MRP4	AASQILILK	light	478.811	399.26	66	26.1	
MRP4	AASQILILK	light	478.811	235.173	66	26.1	
MRP4	AASQILILK	light	478.811	456.282	66	26.1	
MRP4	AASQILILK	light	478.811	200.134	66	26.1	
MRP4	AASQILILK	heavy	482.818	268.211	66	26.1	
MRP4	AASQILILK	heavy	482.818	368.265	66	26.1	
MRP4	AASQILILK	heavy	482.818	403.267	66	26.1	
MRP4	AASQILILK	heavy	482.818	239.18	66	26.1	
MRP4	AASQILILK	heavy	482.818	460.289	66	26.1	
MRP4	AASQILILK	heavy	482.818	204.141	66	26.1	
MRP4	SSLISALFR	light	497.29	435.271	67.4	26.8	
MRP4	SSLISALFR	light	497.29	297.174	67.4	26.8	
MRP4	SSLISALFR	light	497.29	802.482	67.4	26.8	
MRP4	SSLISALFR	light	497.29	489.282	67.4	26.8	
MRP4	SSLISALFR	light	497.29	532.288	67.4	26.8	
MRP4	SSLISALFR	light	497.29	348.167	67.4	26.8	
MRP4	SSLISALFR	heavy	502.294	445.28	67.4	26.8	
MRP4	SSLISALFR	heavy	502.294	302.178	67.4	26.8	
MRP4	SSLISALFR	heavy	502.294	812.49	67.4	26.8	

MRP4	SSLISALFR	heavy	502.294	499.29	67.4	26.8
MRP4	SSLISALFR	heavy	502.294	542.296	67.4	26.8
MRP4	SSLISALFR	heavy	502.294	358.175	67.4	26.8
OATP2B1	SSPAVEQQLLVSGPGK		798.9	1155.6, 1026.6, 711.9	89.4	37.6
OATP2B1	VLAVTDSPAR		514.8	816.4, 745.4, 646.3	68.6	27.4

Supplementary Table S4: LC conditions for furosemide quantification.

Column	UPLC column (Acquity UPLC HSS T3 1.8 µm, 2.1 x 100 mm, Waters			
Guard column	Security Guard column (C18, 4 mm x 2.0 mm, Phenomenex)			
Run Time	4.00 min			
Injection volume	5 µl			
Column oven temperature	40 °C			
Autosampler temperature	5 °C			
Gradient Table:				
Time	Flow Rate	%A	%B	Curve
Initial	0.300	75.0	25.0	Initial
0.5	0.300	75.0	25.0	6
1.8	0.300	5.0	95.0	6
2.7	0.300	5.0	95.0	6
2.8	0.300	75.0	25.0	6
4.0	0.300	75.0	25.0	6
A = 0.1% formic acid water; B = 0.1% formic acid acetonitrile				

Supplementary Table S5: Input parameters used for probenecid (OAT3 inhibitor)

PBPK parameter	Value	Method/reference(s)
1. Physico-chemical and binding		
Molecular mass (g/mol)	285.36	Simcyp library
LogP	3.2	Simcyp library
pKa	3.4	Simcyp library
B/P ratio	0.6	Simcyp library
fu, plasma	0.1	Simcyp library
2. Absorption	ADAM model	
$P_{eff,\ human}$ ($*10^{-6}$ cm/s)	1.73	Simcyp library
fa	0.88	Simcyp library
Ka (hr-1)	0.76	Simcyp library
3. Distribution	Full PBPK model	
Vss (L/kg)	0.11	Method 2[47]
4. Elimination		
CL_{IV} (L/hr)	1.03	Observed[67]
CL_r (L/hr)	0.1	Observed[68]
OAT3 inhibition		
K_i (µM)	3.0	Experimental

Supplementary Table S6: Protein abundance of efflux transporters and %inside-out data in membrane vesicles and transfected cells

Transporter	Protein abundance (pmol/mg protein)	% inside-out vesicles
BCRP	11.4 (vesicles)	32.6
MRP4	0.29 (vesicles)	21.2
OATP2B1	4.25 (cells)	N/A

BIBLIOGRAPHY

(1) Laughon, M. M.; Chantala, K.; Aliaga, S.; Herring, A. H.; Hornik, C. P.; Hughes, R.; Clark, R. H.; Smith, P. B. Diuretic Exposure in Premature Infants from 1997 to 2011. *Am. J. Perinatol.* **2015**, *32* (1), 49–56. https://doi.org/10.1055/s-0034-1373845.

(2) Ponto, L. L.; Schoenwald, R. D. Furosemide (Frusemide). A Pharmacokinetic/Pharmacodynamic Review (Part I). *Clin. Pharmacokinet.* **1990**, *18* (5), 381–408. https://doi.org/10.2165/00003088-199018050-00004.

(3) Ponto, L. L.; Schoenwald, R. D. Furosemide (Frusemide). A Pharmacokinetic/Pharmacodynamic Review (Part II). *Clin. Pharmacokinet.* **1990**, *18* (6), 460–471. https://doi.org/10.2165/00003088-199018060-00003.

(4) Haas, M.; Forbush, B. The Na-K-Cl Cotransporter of Secretory Epithelia. *Annu. Rev. Physiol.* **2000**, *62*, 515–534. https://doi.org/10.1146/annurev.physiol.62.1.515.

(5) Shankar, S. S.; Brater, D. C. Loop Diuretics: From the Na-K-2Cl Transporter to Clinical Use. *Am. J. Physiol. Renal Physiol.* **2003**, *284* (1), F11-21. https://doi.org/10.1152/ajprenal.00119.2002.

(6) Odlind, B. Relationship between Tubular Secretion of Furosemide and Its Saluretic Effect. *J. Pharmacol. Exp. Ther.* **1979**, *208* (3), 515–521.

(7) Ross, B. S.; Pollak, A.; Oh, W. The Pharmacologic Effects of Furosemide Therapy in the Low-Birth-Weight Infant. *J. Pediatr.* **1978**, *92* (1), 149–152. https://doi.org/10.1016/S0022-3476(78)80098-5.

(8) Eades, S. K.; Christensen, M. L. The Clinical Pharmacology of Loop Diuretics in the

Pediatric Patient. *Pediatr. Nephrol.* **1998**, *12* (7), 603–616.

(9) Prandota, J. Clinical Pharmacology of Furosemide in Children: A Supplement. *Am. J. Ther. 8* (4), 275–289.

(10) Engle, M. A.; Lewy, J. E.; Lewy, P. R.; Metcoff, J. The Use of Furosemide in the Treatment of Edema in Infants and Children. *Pediatrics* **1978**, *62* (5), 811–818.

(11) Product Information: Furosemide Oral Solution, Furosemide Oral Solution. Wockhardt USA LLC (per DailyMed), Parsippany, NJ 2015.

(12) Product Information: LASIX(R) Oral Tablets, Furosemide Oral Tablets. sanofi-aventis U.S. LLC (per FDA), Bridgewater, NJ 2016.

(13) Rossano, J. W.; Cabrera, A. G.; Jefferies, J. L.; Naim, M. P. H. M. Y.; Humlicek, T. Pediatric Cardiac Intensive Care Society 2014 Consensus Statement: Pharmacotherapies in Cardiac Critical Care Chronic Heart Failure. *Pediatr. Crit. Care Med.* **2016**, *17* (3 Suppl 1), S20-34. https://doi.org/10.1097/PCC.0000000000000624.

(14) Greenblatt, D. J.; Duhme, D. W.; Allen, M. D.; Koch-Weser, J. Clinical Toxicity of Furosemide in Hospitalized Patients. A Report from the Boston Collaborative Drug Surveillance Program. *Am. Heart J.* **1977**, *94* (1), 6–13. https://doi.org/10.1016/s0002-8703(77)80337-2.

(15) Sica, D. A. Diuretic Use in Renal Disease. *Nature Reviews Nephrology*. February 2012, pp 100–109. https://doi.org/10.1038/nrneph.2011.175.

(16) Tamargo, J.; Segura, J.; Ruilope, L. M. Diuretics in the Treatment of Hypertension. Part 2: Loop Diuretics and Potassium-Sparing Agents. *Expert Opinion on Pharmacotherapy*. Informa Healthcare 2014, pp 605–621. https://doi.org/10.1517/14656566.2014.879117.

(17) Gallagher, K. L.; Jones, J. K. Furosemide-Induced Ototoxicity. *Ann. Intern. Med.* **1979**, *91* (5), 744–745. https://doi.org/10.7326/0003-4819-91-5-744.

(18) DeVito, J. M.; Vance, J. R. Furosemide-Associated Ototoxicity. *Clin. Pharm. 2* (6), 507–508.

(19) Wang, L. A.; Smith, P. B.; Laughon, M.; Goldberg, R. N.; Ku, L. C.; Zimmerman, K. O.; Balevic, S.; Clark, R. H.; Benjamin, D. K.; Greenberg, R. G.; et al. Prolonged Furosemide Exposure and Risk of Abnormal Newborn Hearing Screen in Premature Infants. *Early Hum. Dev.* **2018**, *125*, 26–30. https://doi.org/10.1016/j.earlhumdev.2018.08.009.

(20) FDA Label https://www.accessdata.fda.gov/drugsatfda_docs/label/2010/016273s061lbl.pdf.

(21) Kelly, M. R.; Cutler, R. E.; Forrey, A. W.; Kimpel, B. M. Pharmacokinetics of Orally Administered Furosemide. *Clin. Pharmacol. Ther.* **1974**, *15* (2), 178–186.

(22) Rupp, W. Pharmacokinetics and Pharmacodynamics of Lasix. *Scott. Med. J.* **1974**, *19 Suppl 1*, 5–13. https://doi.org/10.1177/00369330740190S103.

(23) Hammarlund, M. M.; Paalzow, L. K.; Odlind, B. Pharmacokinetics of Furosemide in Man after Intravenous and Oral Administration. Application of Moment Analysis. *Eur. J. Clin. Pharmacol.* **1984**, *26* (2), 197–207. https://doi.org/10.1007/bf00630286.

(24) Vree, T. B.; van den Biggelaar-Martea, M.; Verwey-van Wissen, C. P. Probenecid Inhibits the Renal Clearance of Frusemide and Its Acyl Glucuronide. *Br. J. Clin. Pharmacol.* **1995**, *39* (6), 692–695.

(25) Smith, D. E.; Gee, W. L.; Brater, D. C.; Lin, E. T.; Benet, L. Z. Preliminary Evaluation of Furosemide-Probenecid Interaction in Humans. *J. Pharm. Sci.* **1980**, *69* (5), 571–575.

https://doi.org/10.1002/jps.2600690526.

(26) Kerdpin, O.; Knights, K. M.; Elliot, D. J.; Miners, J. O. In Vitro Characterisation of Human Renal and Hepatic Frusemide Glucuronidation and Identification of the UDP-Glucuronosyltransferase Enzymes Involved in This Pathway. *Biochem. Pharmacol.* **2008**, *76* (2), 249–257. https://doi.org/10.1016/j.bcp.2008.04.014.

(27) Sweetman, S. C. Martindale The Complete Drug Reference 36th. *Pharm. Press* **2009**, No. Press, London, 1140, 1150.

(28) Granero, G. E.; Longhi, M. R.; Mora, M. J.; Junginger, H. E.; Midha, K. K.; Shah, V. P.; Stavchansky, S.; Dressman, J. B.; Barends, D. M. Biowaiver Monographs for Immediate Release Solid Oral Dosage Forms: Furosemide. *Journal of Pharmaceutical Sciences*. John Wiley and Sons Inc. 2010, pp 2544–2556. https://doi.org/10.1002/jps.22030.

(29) Andreasen, F.; Botker, H.; Lorentzen, K. In Vitro Studies on the Hydrolysis of Frusemide in Gastrointestinal Juices. *Br. J. Clin. Pharmacol.* **1982**, *14* (2), 306–309. https://doi.org/10.1111/j.1365-2125.1982.tb01984.x.

(30) Lennernäs, H. Human Intestinal Permeability. *J. Pharm. Sci.* **1998**, *87* (4), 403–410. https://doi.org/10.1021/js970332a.

(31) Ebner, T.; Ishiguro, N.; Taub, M. E. The Use of Transporter Probe Drug Cocktails for the Assessment of Transporter-Based Drug-Drug Interactions in a Clinical Setting-Proposal of a Four Component Transporter Cocktail. *J. Pharm. Sci.* **2015**, *104* (9), 3220–3228. https://doi.org/10.1002/jps.24489.

(32) Rege, B. D.; Yu, L. X.; Hussain, A. S.; Polli, J. E. Effect of Common Excipients on Caco-2 Transport of Low-Permeability Drugs. *J. Pharm. Sci.* **2001**, *90* (11), 1776–1786.

https://doi.org/10.1002/jps.1127.

(33) Al-Mohizea, A. M. Influence of Intestinal Efflux Pumps on the Absorption and Transport of Furosemide. *Saudi Pharm. J.* **2010**, *18* (2), 97–101. https://doi.org/10.1016/j.jsps.2010.02.005.

(34) Beermann, B.; Midskov, C. Reduced Bioavailability and Effect of Furosemide given with Food. *Eur. J. Clin. Pharmacol.* **1986**, *29* (6), 725–727. https://doi.org/10.1007/bf00615967.

(35) McCrindle, J. L.; Li Kam Wa, T. C.; Barron, W.; Prescott, L. F. Effect of Food on the Absorption of Frusemide and Bumetanide in Man. *Br. J. Clin. Pharmacol.* **1996**, *42* (6), 743–746. https://doi.org/10.1046/j.1365-2125.1996.00494.x.

(36) Otsuka, K.; Wagner, C.; Selen, A.; Dressman, J. Prediction of In-Vivo Pharmacokinetic Profile for Immediate and Modified Release Oral Dosage Forms of Furosemide Using an in-Vitro-in-Silico-in-Vivo Approach. *J. Pharm. Pharmacol.* **2015**, *67* (5), 651–665. https://doi.org/10.1111/jphp.12365.

(37) Schlender, J.-F.; Meyer, M.; Thelen, K.; Krauss, M.; Willmann, S.; Eissing, T.; Jaehde, U. Development of a Whole-Body Physiologically Based Pharmacokinetic Approach to Assess the Pharmacokinetics of Drugs in Elderly Individuals. *Clin. Pharmacokinet.* **2016**, *55* (12), 1573–1589. https://doi.org/10.1007/s40262-016-0422-3.

(38) Järvinen, E.; Deng, F.; Kidron, H.; Finel, M. Efflux Transport of Estrogen Glucuronides by Human MRP2, MRP3, MRP4 and BCRP. *J. Steroid Biochem. Mol. Biol.* **2018**, *178*, 99–107. https://doi.org/10.1016/j.jsbmb.2017.11.007.

(39) Li, C. Y.; Basit, A.; Gupta, A.; Gáborik, Z.; Kis, E.; Prasad, B. Major Glucuronide

Metabolites of Testosterone Are Primarily Transported by MRP2 and MRP3 in Human Liver, Intestine and Kidney. *J. Steroid Biochem. Mol. Biol.* **2019**, *191*. https://doi.org/10.1016/j.jsbmb.2019.03.027.

(40) Prasad, B.; Johnson, K.; Billington, S.; Lee, C.; Chung, G. W.; Brown, C. D. A.; Kelly, E. J.; Himmelfarb, J.; Unadkat, J. D. Abundance of Drug Transporters in the Human Kidney Cortex as Quantified by Quantitative Targeted Proteomics. *Drug Metab. Dispos.* **2016**, *44* (12), 1920–1924. https://doi.org/10.1124/dmd.116.072066.

(41) Wang, L.; Prasad, B.; Salphati, L.; Chu, X.; Gupta, A.; Hop, C. E. C. A.; Evers, R.; Unadkat, J. D. Interspecies Variability in Expression of Hepatobiliary Transporters across Human, Dog, Monkey, and Rat as Determined by Quantitative Proteomics. *Drug Metab. Dispos.* **2015**, *43* (3), 367–374. https://doi.org/10.1124/dmd.114.061580.

(42) Lee, M. G.; Chen, M. L.; Chiou, W. L. Pharmacokinetics of Drugs in Blood II. Unusual Distribution and Storage Effect of Furosemide. *Res. Commun. Chem. Pathol. Pharmacol.* **1981**, *34* (1), 17–28.

(43) Cutler, R. E.; Blair, A. D. Clinical Pharmacokinetics of Frusemide. *Clin. Pharmacokinet.* **1979**, *4* (4), 279–296. https://doi.org/10.2165/00003088-197904040-00002.

(44) Andreasen, F.; Mikkelsen, E. Distribution, Elimination and Effect of Furosemide in Normal Subjects and in Patients with Heart Failure. *Eur. J. Clin. Pharmacol.* **1977**, *12* (1), 15–22. https://doi.org/10.1007/bf00561400.

(45) Verbeeck, R. K.; Patwardhan, R. V; Villeneuve, J. P.; Wilkinson, G. R.; Branch, R. A. Furosemide Disposition in Cirrhosis. *Clin. Pharmacol. Ther.* **1982**, *31* (6), 719–725. https://doi.org/10.1038/clpt.1982.101.

(46) Keller, E.; Hoppe-Seyler, G.; Mumm, R.; Schollmeyer, P. Influence of Hepatic Cirrhosis and End-Stage Renal Disease on Pharmacokinetics and Pharmacodynamics of Furosemide. *Eur. J. Clin. Pharmacol.* **1981**, *20* (1), 27–33. https://doi.org/10.1007/BF00554663.

(47) Rodgers, T.; Rowland, M. Physiologically Based Pharmacokinetic Modelling 2: Predicting the Tissue Distribution of Acids, Very Weak Bases, Neutrals and Zwitterions. *J. Pharm. Sci.* **2006**, *95* (6), 1238–1257. https://doi.org/10.1002/jps.20502.

(48) Odlind, B.; Beermann, B. Renal Tubular Secretion and Effects of Furosemide. *Clin. Pharmacol. Ther.* **1980**, *27* (6), 784–790. https://doi.org/10.1038/clpt.1980.111.

(49) Shen, H.; Holenarsipur, V. K.; Mariappan, T. T.; Drexler, D. M.; Cantone, J. L.; Rajanna, P.; Gautam, S. S.; Zhang, Y.; Gan, J.; Shipkova, P. A.; et al. Evidence for the Validity of Pyridoxic Acid (PDA) as a Plasma-Based Endogenous Probe for OAT1 and OAT3 Function in Healthy Subjects. *J. Pharmacol. Exp. Ther.* **2019**, *368* (1), 136–145. https://doi.org/10.1124/jpet.118.252643.

(50) Hasegawa, M.; Kusuhara, H.; Adachi, M.; Schuetz, J. D.; Takeuchi, K.; Sugiyama, Y. Multidrug Resistance-Associated Protein 4 Is Involved in the Urinary Excretion of Hydrochlorothiazide and Furosemide. *J. Am. Soc. Nephrol.* **2007**, *18* (1), 37–45. https://doi.org/10.1681/ASN.2005090966.

(51) Wang, Y.; Li, J.; Herberger, A. L.; Allen, S. M.; Li, L.; Huang, Y.; Rush, A.; Owen, A. J.; Bhoopathy, S.; Hidalgo, I. J. Development of Cell-Based Assays for Assessing Drug Interactions with Human Renal Transporters. *AAPS Drug Transp.* 4.

(52) Andreasen, F.; Hansen, U.; Husted, S. E.; Jansen, J. A. The Pharmacokinetics of

Frusemide Are Influenced by Age. *Br. J. Clin. Pharmacol.* **1983**, *16* (4), 391–397. https://doi.org/10.1111/j.1365-2125.1983.tb02183.x.

(53) Bragatto, M. S.; dos Santos, M. B.; Pinto, A. M. P.; Gomes, E.; Angonese, N. T.; Viezzer, W. F. G.; Donaduzzi, C. M.; Manfio, J. L. Comparison between Pharmacokinetic and Pharmacodynamic of Single- Doses of Furosemide 40 Mg Tablets. *J. Bioequivalence Bioavailab.* **2011**, *3* (8), 191–197.

(54) Shugarts, S.; Benet, L. Z. The Role of Transporters in the Pharmacokinetics of Orally Administered Drugs. *Pharmaceutical Research*. September 2009, pp 2039–2054. https://doi.org/10.1007/s11095-009-9924-0.

(55) Flanagan, S. D.; Cummins, C. L.; Susanto, M.; Liu, X.; Takahashi, L. H.; Benet, L. Z. Comparison of Furosemide and Vinblastine Secretion from Cell Lines Overexpressing Multidrug Resistance Protein (P-Glycoprotein) and Multidrug Resistance-Associated Proteins (MRP1 and MRP2). *Pharmacology* **2002**, *64* (3), 126–134. https://doi.org/10.1159/000056161.

(56) Waller, E. S.; Massarella, J. W.; Tomkiw, M. S.; Smith, R. V; Doluisio, J. T. Pharmacokinetics of Furosemide after Three Different Single Oral Doses. *Biopharm. Drug Dispos. 6* (2), 109–117.

(57) Waller, E. S.; Crismon, M. L.; Smith, R. V; Bauza, M. T.; Doluisio, J. T. Comparative Bioavailability of Furosemide from Solution and 40 Mg Tablets with Different Dissolution Characteristics Following Oral Administration in Normal Men. *Biopharm. Drug Dispos. 9* (2), 211–218.

(58) Vaidyanathan, S.; Bartlett, M.; Dieterich, H. A.; Yeh, C. M.; Antunes, A.; Howard, D.;

Dole, W. P. Pharmacokinetic Interaction of the Direct Renin Inhibitor Aliskiren with Furosemide and Extended-Release Isosorbide-5-Mononitrate in Healthy Subjects. *Cardiovasc. Ther.* **2008**, *26* (4), 238–246. https://doi.org/10.1111/j.1755-5922.2008.00058.x.

(59) Shen, Z.; Yeh, L.-T.; Wallach, K.; Zhu, N.; Kerr, B.; Gillen, M. In Vitro and In Vivo Interaction Studies Between Lesinurad, a Selective Urate Reabsorption Inhibitor, and Major Liver or Kidney Transporters. *Clin. Drug Investig.* **2016**, *36* (6), 443–452. https://doi.org/10.1007/s40261-016-0386-y.

(60) Ayalasomayajula, S.; Schuehly, U.; Pal, P.; Chen, F.; Zhou, W.; Sunkara, G.; Langenickel, T. H. Effect of the Angiotensin Receptor–Neprilysin Inhibitor Sacubitril/Valsartan on the Pharmacokinetics and Pharmacodynamics of a Single Dose of Furosemide. *Br. J. Clin. Pharmacol.* **2018**, *84* (5), 926–936. https://doi.org/10.1111/bcp.13505.

(61) Yamamoto, S.; Kosugi, Y.; Hirabayashi, H.; Moriwaki, T. Impact of P-Glycoprotein on Intestinal Absorption of an Inhibitor of Apoptosis Protein Antagonist in Rats: Mechanisms of Nonlinear Pharmacokinetics and Food Effects. *Pharm. Res.* **2018**, *35* (10). https://doi.org/10.1007/s11095-018-2470-x.

(62) Berthier, J.; Arnion, H.; Saint-Marcoux, F.; Picard, N. Multidrug Resistance-Associated Protein 4 in Pharmacology: Overview of Its Contribution to Pharmacokinetics, Pharmacodynamics and Pharmacogenetics. *Life Sciences*. Elsevier Inc. August 15, 2019. https://doi.org/10.1016/j.lfs.2019.06.015.

(63) Alvan, G.; Helleday, L.; Lindholm, A.; Sanz, E.; Villen, T. Diuretic Effect and Diuretic

Efficiency after Intravenous Dosage of Frusemide [See Comments]. *Br. J. Clin. Pharmacol.* **1990**, *29* (2), 215–219. https://doi.org/10.1111/j.1365-2125.1990.tb03622.x.

(64) De Denus, S.; Rouleau, J. L.; Mann, D. L.; Huggins, G. S.; Cappola, T. P.; Shah, S. H.; Keleti, J.; Zada, Y. F.; Provost, S.; Bardhadi, A.; et al. A Pharmacogenetic Investigation of Intravenous Furosemide in Decompensated Heart Failure: A Meta-Analysis of Three Clinical Trials. *Pharmacogenomics J.* **2017**, *17* (2), 192–200. https://doi.org/10.1038/tpj.2016.4.

(65) Stopfer, P.; Giessmann, T.; Hohl, K.; Sharma, A.; Ishiguro, N.; Taub, M. E.; Zimdahl-Gelling, H.; Gansser, D.; Wein, M.; Ebner, T.; et al. Pharmacokinetic Evaluation of a Drug Transporter Cocktail Consisting of Digoxin, Furosemide, Metformin, and Rosuvastatin. *Clin. Pharmacol. Ther.* **2016**, *100* (3), 259–267. https://doi.org/10.1002/cpt.406.

(66) Stopfer, P.; Giessmann, T.; Hohl, K.; Hutzel, S.; Schmidt, S.; Gansser, D.; Ishiguro, N.; Taub, M. E.; Sharma, A.; Ebner, T.; et al. Optimization of a Drug Transporter Probe Cocktail: Potential Screening Tool for Transporter-Mediated Drug-Drug Interactions. *Br. J. Clin. Pharmacol.* **2018**, *84* (9), 1941–1949. https://doi.org/10.1111/bcp.13609.

(67) Emanuelsson, B. M.; Beermann, B.; Paalzow, L. K. Non-Linear Elimination and Protein Binding of Probenecid. *Eur. J. Clin. Pharmacol.* **1987**, *32* (4), 395–401. https://doi.org/10.1007/BF00543976.

(68) Cunningham, R. F.; Israili, Z. H.; Dayton, P. G. Clinical Pharmacokinetics of Probenecid. *Clin. Pharmacokinet. 6* (2), 135–151. https://doi.org/10.2165/00003088-198106020-00004.